3D printing of ceramic implants

Elke Vorndran, Claus Moseke, and Uwe Gbureck

Three-dimensional powder printing (3DP) is attractive for the direct fabrication of bioceramic implants and scaffolds from a computer aided design file for bone tissue engineering by localized deposition of a reactive binder liquid onto thin powder layers. This article reviews recent findings on novel material developments for the three-dimensional (3D) printing process using either sintering regimes or cement setting reactions. Customized ceramic implants can be fabricated by 3DP using computer tomography data obtained from a patient, whereas further drug modification of such implants can be achieved either *in situ* or post-printing. The excellent biological *in vitro* and *in vivo* behavior of 3D-printed bioceramics together with processing at ambient conditions may give the opportunity to directly produce cell-seeded patient-specific implants for accelerated and enhanced bone regeneration in the future.

Introduction

The primary function of the skeleton is its role as supporting tissue in the human body. The specific hierachic structure of bone (**Figure 1**) is essential for the unique mechanical properties of bone. The combination of organic and inorganic components provides bone with an extreme resistance against tension, compressive, and bending stress, as well as torsion. The architecture of bone tissue comprises the outer periosteum followed by the dense cortical bone and the inner porous cancellous bone. Bone tissue consists of bone cells (osteoblasts, osteoclasts, and osteocytes) embedded into the bone matrix, which is composed of approximately 60–70% inorganic hydroxyapatite, 20% organic compounds (collagen, osteocalcin, proteoglycans), and 10% water.[1] Bone is a slow-growing tissue with only a limited self-healing capacity. Bone defects, caused by disease or trauma, which extend to a critical size >10 mm show no structural bone regeneration but ingrowth of fibrous tissue.[2] To avoid this, bone grafts have to be implanted in such defects to fill the space during the healing and regeneration process. Diverse clinical pictures like infantile craniofacial anomalies, trauma, or cancer can cause cranial or maxillofacial bone defects, which often further extend this critical size. Such bone grafting procedures are being performed worldwide for several million patients per year,[3] at a cost of more than $2 billion.[4]

Although the gold standard in terms of healing success is still the transplantation of autologous grafts obtained from the same individual[5] (for non-load-bearing implants), this is associated with several disadvantages, such as donor site morbidity, limited availability, and the risk of unpredictable resorption (dissolution of bone structure) without bone defect regeneration. Non-autologous bone grafts obtained from a donor have potential infectious and immunological risks. In contrast, alloplastic bone replacement materials (e.g., polymeric or ceramic cements) have the advantage of unlimited availability and consistent material quality; the materials predominantly used in craniomaxillofacial surgery are titanium alloys,[6] calcium phosphate cements, and ceramics[7] as well as different polymers, such as acrylic bone cement and polyetheretherketones.[8] At the moment, only 15% of the global bone graft market consists of synthetic materials, but due to its high growth rate, the commercial significance of this market segment is expected to increase approximately 15% p.a.[9]

While small bone defects can often be treated by intraoperatively formed alloplastic materials (e.g., polymeric or ceramic cements), large and/or geometrically complex defects often require pre-formed implants made by using an individual life-size model or by using layer-by-layer additive manufacturing or three-dimensional (3D) printing techniques. Engineering approaches to create individualized patient-specific implants

Elke Vorndran, Department for Functional Materials in Medicine and Dentistry, University of Würzburg, Germany; elke.vorndran@fmz.uni-wuerzburg.de
Claus Moseke, Department for Functional Materials in Medicine and Dentistry, University of Würzburg, Germany; claus.moseke@fmz.uni-wuerzburg.de
Uwe Gbureck, Department for Functional Materials in Medicine and Dentistry, University of Würzburg, Germany; uwe.gbureck@fmz.uni-wuerzburg.de
DOI: 10.1557/mrs.2015.326

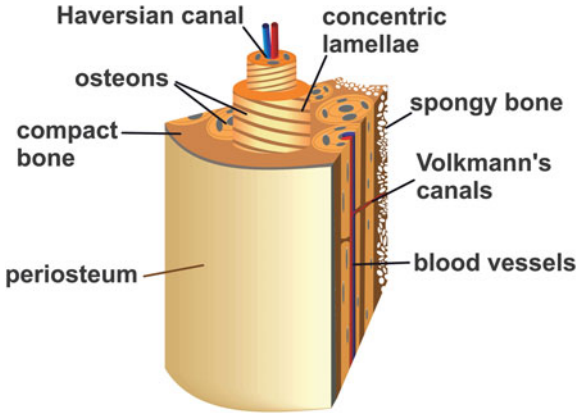

Figure 1. Schematic presentation of the hierarchic structure of bone: The periosteum forms the outer layer of long bones and covers the compact bone. The osteons are concentric cylinders oriented along the main axis of long bones with alternating lamellar substructures. Blood vessels and nerve fibers lie within Haversian and Volkmann's canals and provide for nutrient and oxygen supply as well as for communication between individual bone cells.

(PSI) are based on computer-aided rapid prototyping techniques, which enable a layer-by-layer creation of near-net-shape 3D objects in a wide range of material variations.[10–15] The general underlying principle is spatial control of powder bonding by methods such as selective laser sintering,[16] slip casting,[17] fused deposition modeling,[18–20] stereolithography,[21,22] or 3D powder printing (3DP).[23–25] In particular, 3D printing has captured increasing attention in the past years since it offers the possibility of implant fabrication at room temperature and hence the incorporation of organic, biologically active, or hydrated molecules within the bulk of the implant. This method is suitable to process synthetic bone materials based on calcium or magnesium phosphate ceramics. These materials possess remarkable biocompatibility and bioactivity due to their chemical similarity to the mineral phase of bone. This article aims to review recent progress in 3D printing of customized implants made from ceramics based on calcium or magnesium phosphates, including the design of the implants using computer tomography (CT) data, the development of novel material systems for the printing process, and implant modification with drugs either during fabrication or after the printing process.

Material approaches for 3D printing of bioceramics

Requirements to powder/binder systems

Since the first 3D printer was launched, various material systems have been described for 3D printing purposes, including metals,[26,27] ceramics,[28,29] polymers,[30,31] and composites with applications in many areas, including biomedical engineering. General parameters for controlling the dimensional accuracy of a 3D-printed structure are the particle size distribution, the spreading of the liquid binder in the powder bed, but also the expansion or shrinkage of the structure during the reaction between binder and powder (see the Introductory article in this issue). General requirements for the suitability of a powder/binder system for 3D printing include the possibility to obtain smooth powder layers within the printer for high printing quality and a fast hardening reaction between the powder and printing liquid. The first criterion is associated with the particle size distribution of the powder. It has been demonstrated that ideal particle sizes are in the range of 15–35 µm,[32–35] while a larger size will have detrimental effects on the printing quality, since the particles are then in a similar size range of the layer thickness (80–150 µm). Similarly, powders containing particle fractions with diameters <5 µm generally tend to build up millimeter-sized agglomerates due to van der Waals forces, which leads to the formation of defects and grooves in the powder surface during layer preparation. If small particles <5 µm need to be used in 3DP (e.g., due to higher sintering activity), the powders have to be granulated prior to use in order to meet the previously mentioned size requirements.[36] Alternatively, layer preparation may be performed from powder slurries rather than from dry powders.[33]

A second requirement is a rapid hardening reaction between the binder liquid and the powder. The binder liquid is locally sprayed on the powder bed with a spatial resolution of approximately 20–30 µm for a 600 dots-per-inch print head. The hardening reaction must be fast enough to prevent uncontrolled spreading of the liquid within the porous powder bed, but at the same time must be slow enough to enable the fusion of consecutive powder layers by binder diffusion. Assuming that the next layer is prepared and printed in a typical time frame of 30–60 s, material hardening (and hence binder diffusion) should take place within 1–2 min.

The hardening process in 3DP can be induced by different mechanisms. In one option, the physical hardening mechanism is based on the powders being modified with a polymeric additive (e.g., cellulose, gelatine, starch, or synthetic polymers), which is partially dissolved and will swell when the binder liquid (e.g., water) is applied. A second mechanism uses a chemical reaction between the powder and the binder liquid, for example, the hydraulic reaction between tricalcium phosphate powder with phosphoric acid[37] or tetracalcium phosphate with citric acid solution.[38] The first reaction leads to the formation of brushite ($CaHPO_4{\cdot}2H_2O$) as the setting product,[37,39] while the second cement hardens by the formation of calcium citrates. Other chemical reactions are based on the reaction of polyacrylic acid with chelating ions,[40] the formation of struvite ($NH_4MgPO_4{\cdot}6H_2O$) by reaction of magnesium ions with ammonium phosphate solution,[41] or by a hydraulic reaction between calcium silicates or calcium aluminates with water.[42,43]

Fabrication of high-temperature sintered ceramics and glasses

High-temperature calcium phosphate ceramics such as hydroxyapatite (HA), ß-tricalcium phosphate (β-TCP),

or tetracalcium phosphate are preferably fabricated using organic binders (either added to the powder or dissolved in the printing liquid), which are burnt out after printing (**Table I**). In most cases, the application of the binder does not change the Ca:P ratio of the starting powder, such that after binder burnout and sintering, the final phase composition of the printed sample is similar to the starting powder. When using phosphate-containing binders (e.g., phosphoric acid), a decrease in the Ca:P ratio of the starting powder will occur and hence the phase composition after sintering will change to minerals with lower Ca:P ratios, such as ß-TCP. For example, Castilho et al.[36] produced biphasic HA/ß-TCP ceramics with a dimensional accuracy of >96.5% and a compressive strength of 0.4–1.8 MPa by using calcium phosphate raw powders with a Ca:P ratio of 1.65–2.00 and phosphoric acid as the binder. When the Ca:P ratio is far below 1.5 (e.g., by printing tricalcium phosphate with H_3PO_4), sintering results in the formation of biphasic calcium pyrophosphate/tricalcium phosphate ceramics with glass phase transition at temperatures above 1180°C and an accompanying increase in the compressive strength from 0.8 MPa to 44 MPa.[44]

3D printing of low-temperature phases using reactive cement systems

Reactive cement systems for 3DP can benefit civil engineering as well as biomedical applications (see **Table II**). For example, the former covers the fabrication of casting molds[45] based on magnesium phosphate compounds, while for the biomedical field, low-temperature biominerals such as nanocystalline hydroxyapatite ($Ca_{10}(PO_4)_6(OH)_2$),[37,46,47] brushite ($CaHPO_4{\cdot}2H_2O$), monetite ($CaHPO_4$), or struvite ($NH_4MgPO_4{\cdot}6H_2O$) are processed. Cement setting occurs by a continuous dissolution and reprecipitation reaction, which is initiated by the contact of the aqueous binding liquid with the cement powder. Due to the 3D printing demands for fast solidification, the cement/binder systems have to be highly reactive, but at the same time the particle size has to be relatively large. These detrimental requirements prevent the use of commercially available biocements, which usually have small particle sizes and slow reaction kinetics. A possible solution is the combination of highly reactive calcium phosphates such as α-tricalcium phosphate or tetracalcium phosphate with phosphoric acid as binder. At low

Table I. Examples of material systems used in three-dimensional printing of sintered bioceramic implants.

Powder System	Binder System	Sintering Regime	Material Properties	Ref.
Mixture of small (4 µm) and coarse (50 µm) HA granules with 15 wt% cellulose and starch	Water, 2.5% glycerol, 1% PEG300, 1% Propedal 160; 0.5% polyvinyl alcohol, 0.5% potassium sorbate	1250–1400°C	CS up to 31 MPa at 1400°C; bimodal pore structure with 0.3–0.4 µm intragranular and 20 µm intergranular pores at 1250°C	93
HA (3–5 µm), malto-dextrine (90–100 µm)	Water based (not specified)	1300°C, 1–5 h	Flexural strength = 4.5–12 MPa; porosity 59–64%	94
Tetracalcium phosphate (TTCP), ß-TCP, calcium sulfate <100 µm	25% citric acid	1000–1400°C, 6–24 h	Formation of HA, TTCP, and CaO mixtures after sintering; CS = 0.1–4.3 MPa at a porosity of 36–50%; strength improvement to 76 MPa by polymer infiltration	52
Calcium phosphate granules (HA/ß-TCP) (32–57 µm)	Aqueous solution of 20% dextrin and 2.5% saccharose	1250°C, 2 h	Either pure HA or ß-TCP or biphasic mixture (60:40) of both; CS = 0.6–2.2 MPa; resolution: 150–770 µm	95
Calcium phosphate powder with a Ca:P ratio of 1.65–2.00	10% H_3PO_4	1200°C, 1–15 h	Biphasic mixture of HA and ß-TCP; CS = 0.42–1.81 MPa; microporosity 63–71%; minimum macropore size 300 µm	36
TCP powder doped with 0.25% ZnO or 0.5% SiO_2	Commercial, water-dissolved organic binder	1250°C, 2 h	Predominantly ß-TCP with small amounts of α-TCP; CS = 1.8–5.5 MPa for undoped ceramics increased to 4.3–10.2 MPa with dopants due to improved sintering and densification	96
ß-TCP, bioactive glass ($45SiO_2$, $24.5Na_2O$, $24.5CaO$, $6P_2O_5$), d_{50} = 41 µm	1 M H_3PO_4, 1 M $H_4P_2O_7$, 20% isopropanol	1000°C	CS = 14.9 MPa; resolution: 50 µm	97
Bioactive glass ($6Na_2O$, $12K_2O$, 5MgO, 20CaO, $4P_2O_5$, $53SiO_2$), d_{50} = 3.3–45.8 µm + 6% Dextran	Water–glycerol 7:1	625–1100°C	Formation of crystalline compounds >730°C	98
α/ß-TCP powder (30 µm)	5–30% H_3PO_4	1100–1300°C	Formation of calcium pyrophosphate (CPP) above 350°C and CPP/TCP glass phase above 1280°C; CS = 0.8–44 MPa	44

The final sintering step is intended to remove the organic binder and to improve the mechanical properties of the structure; the final implant composition covers high-temperature calcium phosphate phases such as hydroxyapatite, tricalcium phosphate, or bioactive glasses. HA, hydroxyapatite; TCP, tricalcium phosphate; CS, compressive strength.

Table II. Examples of reactive cement systems used for three-dimensional printing of low-temperature bioceramics by a hydraulic setting reaction.

Powder (particle size)	Binder Liquid	Post-Treatment and Material Properties	Final Setting Product	Ref.
α/ß-$Ca_3(PO_4)_2$ (20–30 µm)	5–30% H_3PO_4	Post-hardening 3 × 30 sec in 20% H_3PO_4	Brushite with residual α/ß-$Ca_3(PO_4)_2$	44
α-$Ca_3(PO_4)_2$ (6.6–50.1 µm)	10% H_3PO_4	–	Not analyzed, but likely brushite	35
$Ca_4(PO_4)_2O$	10% H_3PO_4	Hydrothermal treatment in Na_2HPO_4 solution at 37°C for 7d	Nanocrystalline hydroxyapatite	62
$CaSO_4 \cdot 0.5H_2O$ modified with gelatinized starch; layer thickness 100 µm	Water based	Hydrothermal treatment at 80°C in 1 M Na_2HPO_4 solution 4–24 h	Nanocrystalline hydroxyapatite	47
Mixture of α-$Ca_3(PO_4)_2$ and $Ca_{10}(PO_4)_6(OH)_2$ (30–150 µm sieved fractions)	10–20% H_3PO_4 + 0.25% Tween 80	Flash dipping in 0.1% H_3PO_4	Not analyzed, most likely brushite with residual raw powder	62

pH-values of the acid (approximately 1–2) the compounds react within seconds to form a matrix of brushite with high dimensional accuracy.[48]

$$\alpha\text{-}Ca_3\left(PO_4\right)_2 + H_3PO_4 + 6\,H_2O \rightarrow \quad 3\ CaHPO_4 \cdot 2H_2O. \quad (1)$$

The initially achieved compressive strength of approx. 3–5 MPa of the scaffold can be increased to 23 MPa by repeated immersion in phosphoric acid (post-hardening) due to a higher degree of conversion to brushite. Another highly reactive biocement system is based on the reaction of trimagnesium phosphate (farringtonite) and magnesium oxide powder with ammonium phosphate binder solution.[41] In this case, magnesium ammonium phosphate hexahydrate (struvite) is formed, which results in material properties (resolution, macropore size, strength) similar to the above-mentioned brushite cements. Major advantages of struvite ceramics are their higher solubility (and hence accelerated resorption)[49] and the neutral pH conditions of their setting reaction. The latter is beneficial for their use in drug delivery applications, since the acidic pH of brushite cements is not compatible with delicate protein-based bioactives.

Fabrication and structural properties of 3DP implants

Up to now, the most important application of 3D printing in medicine has been the fabrication of geometrically accurate models for surgery planning. Klammert et al.[50] utilized the 3D printing technique for the fabrication of individual cranial models according to patient data obtained by computed tomography. This method turned out to be much cheaper and faster than the established model-making procedure by stereolithography and was successfully applied in the manufacturing process of individual fixation plates for midface distraction of patients with syndromic malformation (deformities resulting from underlying diseases) of the skull, as well as for the preoperative simulation of the osteotomy lines (which define the intraoperative cutting of the bone).

The fabrication of ceramic PSI in craniomaxillofacial surgery is another possible application of 3DP. Custom-made bioceramic implants would have some benefits, as compared to commonly used titanium implants. Titanium is non-degradable, is not able to serve as a drug delivery system (DDS) and has a thermal conductivity of about two orders of magnitude higher than those of ceramics.[51] The latter is an often largely underestimated parameter; many patients with large-sized craniofacial metal implants suffer from environmental temperature deviations, which are more effectively transported into delicate soft tissue (e.g., the brain) by metal implants rather than by bioceramics or natural bone tissue. Nevertheless, due to the brittleness of ceramic implants, many cases still remain where the use of metal implants is inevitable.

Fabrication of such implants first requires the design of the implant using CT data of the defect.[51] CT scans commonly produce digital imaging and communications in medicine (DICOM) data sets (a management system for the storage and exchange of patient data and pictures) of the bone structure, which can be processed and manipulated by using commercially available software. The virtual generation of the implants (computer-aided design, CAD) is commonly conducted using mirror imaging procedures, followed by manual post-processing and the creation of DICOM files of the implants. Finally the DICOM files have to be converted into a surface tessellation language format (this format describes a 3D object by a triangular representation of the surface geometry), which is required for fabrication in the 3D printer (**Figure 2**). The implant can either be printed directly[51,52] by using the previously mentioned high-temperature ceramic or cement systems (and taking into account the dimensional changes during sintering), or metallic and ceramic molds can be printed, which then are used to obtain personalized implants by self-propagating high-temperature synthesis of β-TCP, respectively hydroxyapatite.[53] The latter fabrication route enabled good control of structure and porosity of the scaffolds with sufficient biomechanical properties for the desired application as a gap filler for the treatment of opening wedge high tibial osteotomy.[53] However, due to the high temperatures involved in the synthesis, the process cannot be used in combination with the incorporation of thermally unstable substances like biologically active agents.

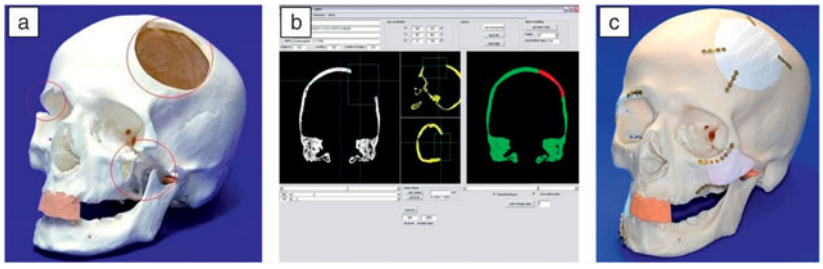

Figure 2. (a) Process chain for the fabrication of patient-specific implants for typical craniomaxillofacial defects by three-dimensional (3D) printing. (b) Implants were designed after digitization of defects by computer tomography analysis (DICOM data file) by using a CAD/CAM algorithm and mirror-imaging of the intact skull side following post operations such as smoothing and the elimination of artifacts. (c) The designed implants were manufactured by 3D printing using calcium phosphate powder and fixed with miniplate osteosynthesis, respectively bicortical osteosynthesis (mandibular defect). Data reprinted with permission from Reference 51. © 2010 Elsevier.

Three-dimensional printing is also used to fabricate calcium phosphate scaffolds with different pore sizes and pore connectivities,[54–57] as shown in **Figure 3**a. Microwave sintering is being applied to enhance the mechanical strength of 3DP β-tricalcium phosphate (β-TCP) scaffolds.[56] Figure 3b shows that the addition of SrO and MgO dopants as well as microwave sintering of β-TCP scaffolds, fabricated with the 3DP method with a designed pore size of 500 μm, led to significantly increased compressive strength. Microwave sintering of the TCP scaffolds improved compressive strength from (6.62 ± 0.67) MPa to (10.95 ± 1.28) MPa, as a result of efficient densification.[56] The presence of dopants as well as microwave sintering further improved compressive strength to (12.01 ± 1.56) MPa.[54]

A general weakness of 3D-printed (porous) bioceramic implants is their brittle nature and relatively low mechanical performance. However, implant pores can be infiltrated with polymers to alter strength, fracture resistance, and biodegradation speed. For example, infiltration with (non-degradable) methacrylate polymers was shown to improve the bending strength of 3DP hydroxyapatite ceramics by nearly two orders of magnitude to >50 MPa.[32] If a reduction of the resorbability is undesired, degradable monomers like dianhydro-D-glucitol[bis(di(lactoyl)methacrylate)] can be used for infiltration, which shows similar effects on the mechanical performance of 3D-printed bioceramic implants.[52]

In vitro and *in vivo* performance

Similar to other ceramic processing routes, 3D-printed calcium orthophosphates like β-TCP and hydroxyapatite were proved to have excellent biocompatibility.[58] However, in applications where the complete resorption of the printed scaffold and its replacement by natural bone tissue is desired, their relatively low chemical solubility may be considered as a disadvantage. In order to take into account cell-biological aspects of 3D-printed implant resorption, Detsch et al. performed *in vitro* studies with murine macrophages (white blood cells of rodents) of the cell line RAW 264.7 and found that both 3D-printed HA and β-TCP as well as biphasic mixtures promoted the differentiation of precursor cells into bone-resorbing osteoclast-like cells. The most promising results were found for a biphasic HA/TCP composition of 60/40, which supported the assumption that the degradation behavior of calcium phosphate scaffolds can be tailored by means of phase composition.[59] The higher chemical solubility of secondary calcium phosphates like brushite and monetite makes them promising alternatives to HA and ß-TCP.

Klammert et al. performed extensive experiments with printed brushite/monetite scaffolds and showed the excellent suitability of the material for 3D printing of highly accurate craniofacial implants,[51] and they found promising results regarding the biocompatibility in osteoblastic cell culture.[60] The biocompatibility of such printed implants was confirmed *in vivo* by Habibovic et al.,[61] who demonstrated that the materials not only provide osteoconductive properties in bone, but were also osteoinductive, as they lead to bone formation *in vivo.* Recently, Inzana et al.[62] published an approach to print scaffolds from HA/α-TCP powders using binders with reduced phosphoric acid concentration. This was achieved by adding the non-toxic surfactant Tween 80 as well as Type I collagen (one of the 28 types of collagen, especially found in bone, tendons, ligaments, dermis, dentin and organ capsules). *In vivo*, these materials showed similar new bone formation as allografts, but the authors pointed out the necessity of further studies, which will have to confirm the ability of such collagen-infiltrated printed scaffolds to fully heal critically sized bone defects.

Surprisingly, 3D-printed monetite implants were found to show better *in vivo* degradation than brushite, although the latter is chemically more soluble.[63] The reason for this was identified to be the formation of a low-soluble HA phase in brushite samples by a dissolution/reprecipitation reaction.[39,64] Torres et al. conducted a study of printed monolithic scaffolds, which were designed for vertical bone augmentation for improved anchorage of dental implants. They used monetite ($CaHPO_4$), which had been found to perform similarly to autologous grafts regarding the vertical bone height gained in previous *in vivo* experiments.[65] Disc-shaped samples with a hole in the middle were 3D printed, which were then screwed onto rabbit calvaria (skullcap). The histological examination of the samples after eight weeks of implantation revealed infiltration of the scaffolds with new bone, but neither necrosis nor foreign body reactions were observed.[66] A follow-up study focused on the design of the monetite grafts and showed that macroporous geometry with pore sizes of 300–400 μm can enhance bone growth. In particular, it was found that the effect of the increased porosity was higher in the implant's region with direct contact to the bone surface.[67]

Increased bone formation and better early bone remodeling (including bone ingrowth within the implant, resorption of

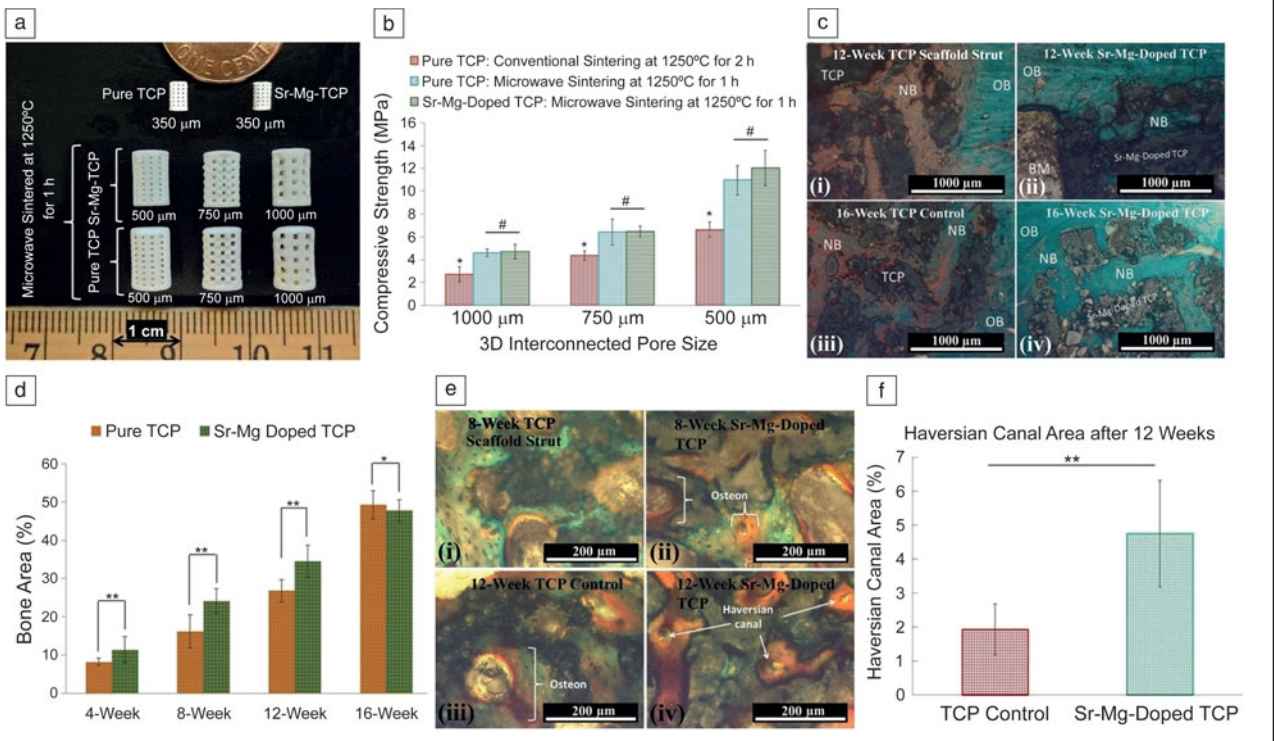

Figure 3. (a) Microwave sintered three-dimensional printed (3DP) tricalcium phosphate (TCP) and Sr-Mg-doped TCP scaffolds;[54,55] (b) their compressive strength comparison (*p <0.05 and #p >0.05, *n* = 10);[55,56] (c) photomicrograph of 3DP pure TCP scaffolds (i and iii), and Sr/Mg-doped TCP scaffolds (ii and iv) showing bone remodeling inside the interconnected macro- and intrinsic micropores of the 3DP scaffolds after 12 and 16 weeks in a rat distal femoral defect model. Modified Masson Goldner's trichrome staining (histological staining technique that allows one to distinguish remnants of synthetic bone substitutes, old bone, and newly formed bone). Dark gray/black = scaffold; orange/red = osteoid; green/bluish = new mineralized bone/old bone.[55] (d) Histomorphometric analysis of bone area fraction (total newly formed bone area/total area, %) (**p <0.05, *p >0.05, *n* = 8);[55] (e) photomicrograph of 3DP pure TCP implants (i and iii), and Sr-Mg-doped TCP implants (ii and iv) showing osteon and Haversian canal formation as part of the bone remodeling process inside the designed interconnected macro and intrinsic micropores of 3DP scaffolds after 8 and 12 weeks in a rabbit femoral condyle defect model (defined implant drill hole in the round bony protrusions from either side of the bottom of thigh bone).[54] Modified Masson Goldner's trichrome staining; (f) histomorphometric analysis of Haversian canal area (Haversian canal area/total area, in %) after 12 weeks (**p <0.05, *n* = 6).[54] OB: old bone, NB: new bone, O: osteoid, and BM: bone marrow. Data reprinted with permission from Reference 55. © 2013 Royal Society of Chemistry; Reference 56. © 2012 Wiley; and Reference 54. © 2014 Wiley.

the implant by osteoclasts, and new bone formation by osteoblasts) were induced by the addition of the dopants SrO and MgO into the 3DP TCP scaffolds, as compared to undoped TCP scaffolds (see Figure 3c–f). The presence of dopants in TCP resulted in increased extracellular matrix formation and accelerated mineralization, when tested in rat femoral defects, as compared to pure TCP.[55] These 3DP doped TCP scaffolds also showed early wound healing by increased osteoid (bone formation), increased osteon, and an enhanced network of blood vessel formation, when implanted in a rabbit femoral condyle defect model (see Figure 3e–f).[54] The presence of 0.5 wt% SiO_2 and 0.25 wt% ZnO in 3DP TCP scaffolds is beneficial for both mechanical and *in vivo* osteogenesis and angiogenesis.[57,58]

Drug delivery applications

Risks and limitations of systemic drug applications, namely side effects due to high plasma concentration, elimination or inactivation of drugs during *in vivo* transport, low bioavailability resulting from low blood supply, or biological barriers of target tissue, can be overcome by local drug administration via DDS.[68] Such DDS are designed for the controlled release of bioactives directly into a defined target tissue in order to maintain a sufficient therapeutic level of the drug over a defined period of time. The modification with biologically active substances could induce specific and localized biological responses like angiogenesis or osteogenesis[69] as well as prevent infections by the addition of antibiotics[70] or the treatment of cancer by chemotherapeutical agents[71] with negligible systemic toxicity.[72]

Recent developments concern the use of printed ceramic scaffolds as DDS.[73–75] Especially for the treatment of bone defects, mechanically stable ceramic implants with controllable geometry and drug eluting properties are therapeutically advantageous. An early study investigated the adsorption behavior of antibiotics on different printed calcium phosphate matrices and the release kinetics resulting from homogeneous drug loading of porous matrices.[73] It was demonstrated that the

release kinetics were predominantly determined by physical properties such as porosity and the specific surface area of the matrices or by drug–matrix interactions. Although differences were noted in adsorption and release profiles between different bioceramics, a sustained release could be achieved by infiltration of the DDS with a degradable polymer.[73,74]

A subsequent *in vivo* study showed that manual application of BMP-2 (bone morphogenetic proteins Type II; a growth factor, which induces the formation of bone and cartilage by stimulating the differentiation of osteoblasts in various cell types) within a 3D-printed hydroxyapatite scaffold enhanced bone growth, as compared to unloaded scaffolds or scaffolds with a delayed BMP-2 application.[75]

Three-dimensional powder printing TCP scaffolds can also be used for local drug delivery of small osteogenic drug molecules or growth factors.[76] **Figure 4** shows alendronate (AD) delivery (a bisphosphonate-based drug, widely used in patients with osteoporosis) from polycaprolactone-coated (PCL-coated) 3DP TCP scaffolds. PCL-coated scaffolds showed more controlled drug release kinetics than those composed of pure TCP. Both polymer–drug chemical interactions and polymer solubility in the release media influence the release kinetics.[76–78] Histomorphology (study of the cell morphology) and its analysis revealed excellent bone formation on PCL-AD-coated 3DP TCP scaffolds.[76]

A more sophisticated fabrication approach for DDS is the use of multicolor 3D printers. This provides an accurate fabrication method with local control over composition, drug load, micro-, and macrostructure. For this process, drugs are dissolved or dispersed in a solution and printed within defined areas of the scaffold, whereas the solutions have to be adjusted to gain optimal printability.[79] Scaffold properties (e.g., porosity, geometry, degradability, and chemical composition) as well as the drug concentration profile within the carrier system are known as determinant factors for drug release. Regulative instruments for these factors are given by the printing parameters like binder composition, the amount of applied binder or drug solution, and precise spatial deposition of single or multiple drug solutions, which can be varied during the printing process.

An early approach of using 3DP as a local drug deposition device was made by Wu et al. in 1996.[80] The authors controlled the release rate of dyes as model drugs from PCL and poly(ethylene oxide) by adjusting the local drug concentration and matrix composition. In subsequent studies, several drug loaded implantable polymeric or cellulosic systems with controlled release patterns of single or multiple drugs were fabricated.[81–84] Wu et al. printed implants for bone tuberculosis treatment from poly(DL-lactic acid) powder in the shape of a multilayer concentric cylinder, in which each layer was loaded with either isoniazid or rifampicin.[85] The combination of the two antibiotics isoniazid and rifampicin is used as a common treatment procedure in the case of tuberculosis. This loading type led to an orderly release of both drugs from the outside to the inside, with peak concentrations at eight to 12-day intervals. Yu et al. investigated the release behavior of acetaminophen from depot-loaded (loading restricted to the core of the structure) ethylcellulose tablets. Release-retarding material gradients and drug-free diffusion barriers were utilized to gain a constant release rate over a period of 5–13 h governed by matrix erosion and diffusion processes.[84] In another study, the authors used the geometry of a doughnut-shaped, cellulosic DDS to regulate the erosion process and with this the release kinetic of the model drug.[86]

The ability to simultaneously and precisely control the geometry of a ceramic scaffold and its drug modification was demonstrated by Vorndran et al.[87] The authors used a commercial multicolor printer for ceramic DDS preparation (**Figure 5**a), in which one print head was used for applying the binder, while the other three channels were filled with different drugs (BMP-2 = growth factor, which induces bone formation; vancomycin = antibiotic; heparin = anticoagulant) or polymer solution (chitosan hydrochloride). A spatial resolution of approximately 300 µm of the drugs within the matrix was achieved by using a cellulose-modified tricalcium phosphate powder. Drug release kinetics were shown to depend on the drug localization (homogeneous, depot,

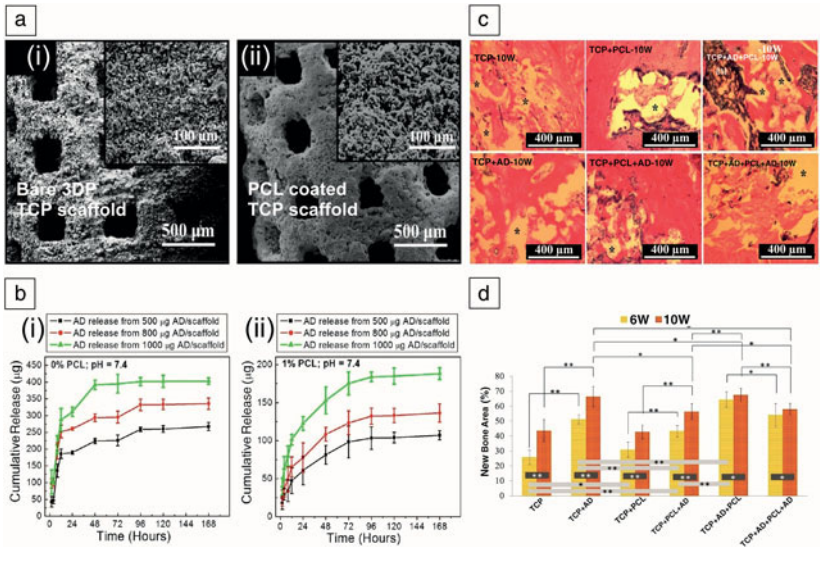

Figure 4. (a) Surface morphology of three-dimensional printed (3DP) (i) bare tricalcium phosphate (TCP) and (ii) polycaprolactone (PCL)-coated 3DP TCP scaffolds; (b) cumulative alendronate (AD) release at pH 7.4 phosphate-buffered saline from (i) bare and (ii) PCL-coated scaffolds. (c) Photomicrographs of representative histological sections after hematoxylin and eosin staining of decalcified tissue sections showing the development of bone formation after 10 weeks. BM = bone marrow; *indicates acellular regions derived from scaffold. (d) Histomorphometric analysis showing total new percent bone formation comparison between different compositions (**p <0.05, *p >0.05, n = 8).[76] Data reprinted with permission from Reference 76. © 2014 American Chemical Society.

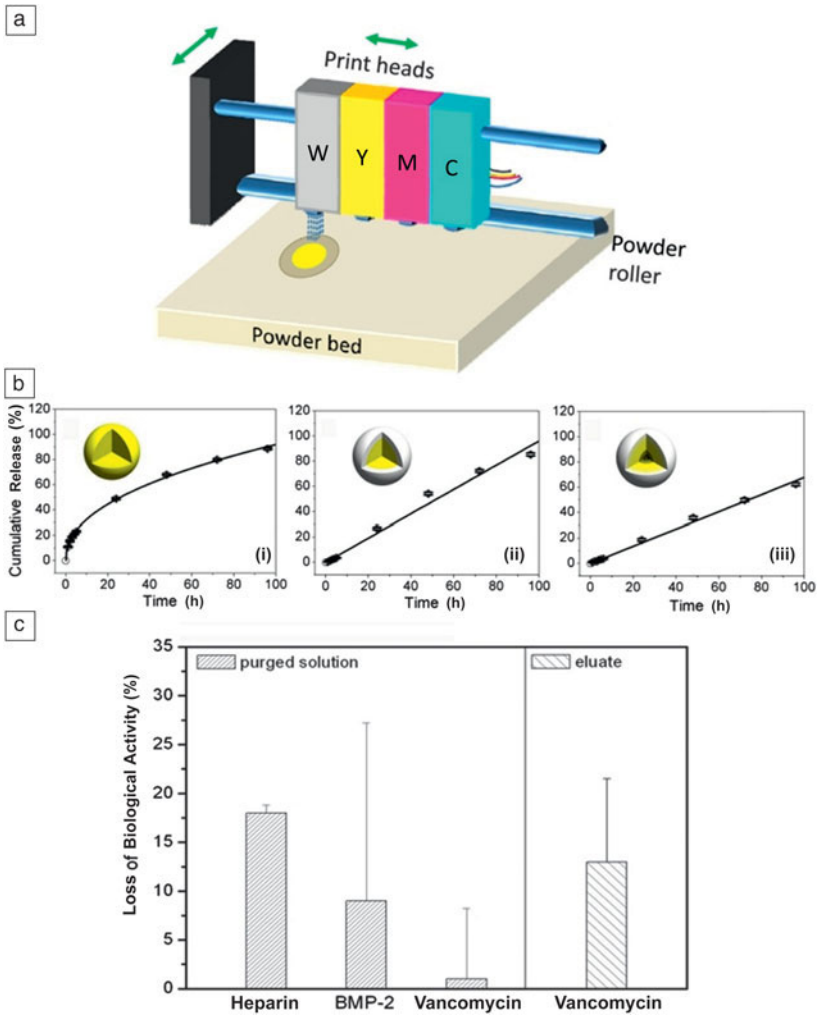

Figure 5. (a) Multicolor three-dimensional powder printer and principle of printing: A thin and smooth powder layer is moved from the powder reservoir to the powder bed. According to the computer data, binder solution is applied through one print head (W) in the corresponding areas, where the solidification of the powder takes place immediately. The local application of various solutions (e.g., polymers, drugs) within the printed structure is possible via additional print heads (Y = yellow, M = magenta, C = cyan). (b) Cumulative release of the model drug vancomycin hydrochloride from printed polymer-modified calcium phosphate spheres. The release profile depends on the drug localization within the structure. (i) Homogeneous drug modification resulted in first-order release kinetics. (ii) Depot and (iii) gradual drug loading resulted in a linear (zero-order) release. (c) Physical and chemical stresses have the potential to deteriorate the biological activity of additives from the fabrication process of brushite samples to biological testing. The purging process reduces biological activities of heparin, BMP-2, and vancomycin. The complete fabrication and release process resulted in a further reduction of the biological activity of vancomycin (eluate). Data reprinted with permission from Reference 87. © 2010 Wiley-VCH.

or gradient) within the scaffolds; while homogeneously loaded scaffolds provided first order release kinetics (Figure 5b(i)), drug depots or gradients resulted in constant release rates over a period of three to four days (Figure 5b(ii)–(iii)) with a loss of biological activity of 13% for vancomycin after incorporation into the ceramic matrix and subsequent *in vitro* release (Figure 5c). To provide a sufficient release of biologically active drugs, the pharmaceutical agents have to be compatible with the physical and chemical conditions during the printing process. Figure 5c presents the loss of biological activity after different processing stages of 3D-printed tricalcium-phosphate-based ceramics for different drugs. The loss of biological activity of printed drug solutions could be attributed to the partial thermal evaporation of the bioactive liquid during purging through the print heads. However, the bulk activity (>82%) could be retained during the purging process even for heat-sensitive proteins such as BMP-2. In the case of tricalcium-phosphate-based ceramics, the processing of drug-loaded structures via 3DP involved contact with the phosphoric acid binder. The eluate of vancomycin obtained after performing the whole printing process followed by *in vitro* release showed an activity of 87%.

Current challenges and future perspectives

Three-dimensional (3D) printing of ceramic implants and scaffolds offer the possibility to fabricate tailored structures with simultaneous control over geometry, porosity, and composition. In addition to traditional material approaches using a sintering reaction as the final manufacturing step, the use of low-temperature setting biocements provides the opportunity to produce hydrated calcium or magnesium phosphates with enhanced degradation ability. In the future, the fabrication process by 3D printing may also be used for direct cell seeding of the scaffolds. Inkjet printing of cells is already a reality.[88,89] It was demonstrated by Xu et al.[90] that the temperature of the binder is increased by only 4–10°C during bubble-jet printing, hence living cells like neuronal, endothelial, and mesodermal stem cells could be printed into pre-fabricated hydrogel scaffolds (collagen, alginate).[91]

Progress in developing low-temperature rapid prototyping systems using a cement setting reaction may open the possibility to fabricate scaffolds of different compositions (ceramic, hydrogel), which are simultaneously loaded with bioactives and seeded with cells at the same time. The major challenge for the incorporation of living cells in cements during 3D printing is probably the chemical environment during setting. The already established brushite-based cements set at pH <2 and are therefore most likely not suitable for direct cell seeding during printing. Alternatives may include either the use of

struvite forming cements with a neutral pH during setting or the encapsulation of the cells in hydrogel particles, such that cells are protected during the cement setting reaction. Such direct cell seeding in biocements has already been established by using alginate encapsulated cells.[92]

A future challenge would be size minimization of the cell-loaded particles to a size <30 μm to ensure printability through a nozzle. Another big challenge is related to the 3D printers themselves, which are commonly designed for engineering applications. However, the fabrication of the previously mentioned drug and cell loaded samples would require a process chain under clean and sterile conditions. This would imply that those parts of the printer in contact with the implant material need to be easily cleaned and sterilized prior to printing, and also the printing process itself has to be performed on a biological work bench. In addition, with increasing complexity of such multistep techniques, the maintenance of reliability and reproducibility becomes an issue of growing significance. These parameters have to be optimized in parallel to the development of the technique itself, in order to create medical products of sustainable quality. Engineering printers that meet these challenging demands will be the next step in the fabrication and clinical application of drug or cell-loaded ceramic implants.

Acknowledgments

The authors would like to acknowledge financial support from the Deutsche Forschungsgemeinschaft (DFG Gb1/7–2 and Gb1/11–2). The authors also acknowledge helpful discussions with Susmita Bose and Amit Bandyopadhyay.

References

1. D. Felsenberg, *Pharm. Unserer Zeit* **30**, 488 (2001).
2. M. Aaboe, E.M. Pinholt, E. Hjorting-Hansen, *Br. J. Oral Maxillofac. Surg.* **33**, 312 (1995).
3. A.S. Greenwald, S.D. Boden, V.M. Goldberg, Y. Khan, C.T. Laurencin, R.N. Rosier, *J. Bone Joint Surg.* **83**, S98 (2001).
4. J.R. Jones, S. Lin, S. Yue, P.D. Lee, J.V. Hanna, M.E. Smith, R.J. Newport, *Proc. Inst. Mech. Eng. H* **224**, 1373 (2010).
5. J.F. Keating, M. McQueen, *J. Bone Joint Surg. Br.* **83**, 3 (2001).
6. H. Eufinger, A.R.M. Wittkampf, M. Wehmöller, F.W. Zonneveld, *J. Cranio-Maxillofac. Surg.* **26**, 373 (1998).
7. H. Siebert, P. Schleier, J. Beinemann, W. Fried, W. Zenk, D. Schumann, *Mund Kiefer Gesichtschir.* **10**, 185 (2006).
8. P. Scolozzi, A. Martinez, B. Jaques, *J. Craniofac. Surg.* **18**, 224 (2007).
9. M. Bohner, *Mater. Today* **13**, 24 (2010).
10. H. Eufinger, M. Wehmöller, E. Machtens, L. Heuser, A. Harders, D. Kruse, *J. Cranio-Maxillofac. Surg.* **23**, 175 (1995).
11. H. Eufinger, C. Rasche, J. Lehmbrock, M. Wehmöller, S. Weihe, I. Schmitz, C. Schiller, M. Epple, *Biomaterials* **28**, 475 (2007).
12. S. Weihe, M. Wehmöller, H. Schliephake, S. Haßfeld, A. Tschakaloff, J. Raczkowsky, H. Eufinger, *Int. J. Oral Maxillofac. Surg.* **29**, 384 (2000).
13. J. Darsell, S. Bose, H.L. Hosick, A. Bandyopadhyay, *J. Am. Ceram. Soc.* **86**, 1076 (2003).
14. D.W. Hutmacher, *Biomaterials* **21**, 2529 (2000).
15. D.W. Hutmacher, *J. Biomater. Sci. Polym. Ed.* **12**, 107 (2001).
16. Z. Sadeghian, J.G. Heinrich, F. Moztarzadeh, *CFI Ceram. Forum Int.* **81**, E39 (2004).
17. C.E. Wilson, J.D. de Bruijn, C.A. van Blitterswijk, A.J. Verbout, W.J.A. Dhert, *J. Biomed. Mater. Res. Part A* **68A**, 123 (2004).
18. M.A. Jafari, W. Han, F. Mohammadi, A. Safari, S.C. Danforth, N. Langrana, *Rapid Prototyp. J.* **6**, 161 (2000).
19. S.J. Kalita, S. Bose, H.L. Hosick, A. Bandyopadhyay, *Mater. Sci. Eng. C* **23**, 611 (2003).
20. E.Y. Teo, S.-Y. Ong, M.S. Khoon Chong, Z. Zhang, J. Lu, S. Moochhala, B. Ho, S.-H. Teoh, *Biomaterials* **32**, 279 (2011).
21. M.L. Griffith, J.W. Halloran, *J. Am. Ceram. Soc.* **79**, 2601 (1996).
22. F.P.W. Melchels, J. Feijen, D.W. Grijpma, *Biomaterials* **31**, 6121 (2010).
23. E.M. Sachs, J.S. Haggerty, M.J. Cima, P.A. Williams, US Patent 5204055 A (April 20, 1993).
24. T.R. Jackson, H. Liu, N.M. Patrikalakis, E.M. Sachs, M.J. Cima, *Mater. Des.* **20**, 63 (1999).
25. A. Butscher, M. Bohner, S. Hofmann, L. Gauckler, R. Müller, *Acta Biomater.* **7**, 907 (2011).
26. K. Lu, W.T. Reynolds, *Powder Technol.* **187**, 11 (2008).
27. M. Chandrasekaran, K. Lim, M. Lee, P. Cheang, *Singap. Inst. Manuf. Technol. (SIMTech) Tech. Rep.* **8**, 1 (2007).
28. B. Leukers, H. Gülkan, S.H. Irsen, S. Milz, C. Tille, M. Schieker, H. Seitz, *J. Mater. Sci. Mater. Med.* **16**, 1121 (2005).
29. P.H. Warnke, H. Seitz, F. Warnke, S.T. Becker, S. Sivananthan, E. Sherry, Q. Liu, J. Wiltfang, T. Douglas, *J. Biomed. Mater. Res. Part B* **93B**, 212 (2010).
30. J. Suwanprateeb, S. Kerdsook, T. Boonsiri, P. Pratumpong, *Polym. Int.* **60**, 758 (2011).
31. J. Suwanprateeb, R. Chumnanklang, *J. Biomed. Mater. Res. Part B* **78B**, 138 (2006).
32. J. Suwanprateeb, R. Sanngam, W. Suwanpreuk, *J. Mater. Sci. Mater. Med.* **19**, 2637 (2008).
33. E. Sachs, US Patent 6036777 A (March 14, 2000).
34. B.Y. Tay, J.R.G. Evans, M.J. Edirisinghe, *Int. Mater. Rev.* **48**, 341 (2003).
35. A. Butscher, M. Bohner, C. Roth, A. Ernstberger, R. Heuberger, N. Doebelin, P. Rudolf von Rohr, R. Müller, *Acta Biomater.* **8**, 373 (2012).
36. M. Castilho, C. Moseke, A. Ewald, U. Gbureck, J. Groll, I. Pires, J. Teßmar, E. Vorndran, *Biofabrication* **6**, 015006 (2014).
37. U. Gbureck, T. Hölzel, C.J. Doillon, F.A. Müller, J.E. Barralet, *Adv. Mater.* **19**, 795 (2007).
38. E. Vorndran, M. Klarner, U. Klammert, L.M. Grover, S. Patel, J.E. Barralet, U. Gbureck, *Adv. Eng. Mater.* **10**, B67 (2008).
39. U. Gbureck, T. Hölzel, U. Klammert, K. Würzler, F.A. Müller, J.E. Barralet, *Adv. Funct. Mater.* **17**, 3940 (2007).
40. A. Pfister, U. Walz, A. Laib, R. Mülhaupt, *Macromol. Mater. Eng.* **290**, 99 (2005).
41. U. Klammert, E. Vorndran, T. Reuther, F.A. Müller, K. Zorn, U. Gbureck, *J. Mater. Sci. Mater. Med.* **21**, 2947 (2010).
42. A.-K. Maier, L. Dezmirean, J. Will, P. Greil, *J. Mater. Sci.* **46**, 2947 (2011).
43. G.J. Gibbons, R. Williams, P. Purnell, E. Farahi, *Adv. Appl. Ceram.* **109**, 287 (2010).
44. U. Gbureck, T. Hölzel, I. Biermann, J.E. Barralet, L.M. Grover, *J. Mater. Sci. Mater. Med.* **19**, 1559 (2008).
45. E. Vorndran, K. Wunder, C. Moseke, I. Biermann, F.A. Müller, K. Zorn, U. Gbureck, *Adv. Appl. Ceram.* **110**, 476 (2011).
46. U. Gbureck, T. Hölzel, R. Thull, F.A. Müller, J.E. Barralet, *Cytotherapy* **8**, 14 (2006).
47. J. Suwanprateeb, W. Suvannapruk, K. Wasoontararat, *J. Mater. Sci. Mater. Med.* **21**, 419 (2010).
48. E. Vorndran, thesis, Würzburg, Germany (2011).
49. B. Kanter, M. Geffers, A. Ignatius, U. Gbureck, *Acta Biomater.* **10**, 3279 (2014).
50. U. Klammert, H. Böhm, T. Schweitzer, K. Würzler, U. Gbureck, J. Reuther, A. Kübler, *J. Cranio-Maxillofac. Surg.* **37**, 210 (2009).
51. U. Klammert, U. Gbureck, E. Vorndran, J. Rödiger, P. Meyer-Marcotty, A.C. Kübler, *J. Cranio-Maxillofac. Surg.* **38**, 565 (2010).
52. A. Khalyfa, S. Vogt, J. Weisser, G. Grimm, A. Rechtenbach, W. Meyer, M. Schnabelrauch, *J. Mater. Sci. Mater. Med.* **18**, 909 (2007).
53. F. Zhim, R.A. Ayers, J.J. Moore, R. Moufarrège, L. Yahia, *J. Biomater. Appl.* **27**, 323 (2012).
54. S. Tarafder, W.S. Dernell, A. Bandyopadhyay, S. Bose, *J. Biomed. Mater. Res. Part B* (2014), doi: 10.1002/jbm.b.33239.
55. S. Tarafder, N.M. Davies, A. Bandyopadhyay, S. Bose, *Biomater. Sci.* **1**, 1250 (2013).
56. S. Tarafder, V.K. Balla, N.M. Davies, A. Bandyopadhyay, S. Bose, *J. Tissue Eng. Regen. Med.* **7**, 631 (2013).
57. S. Bose, M. Roy, A. Bandyopadhyay, *Trends Biotechnol.* **30**, 546 (2012).
58. G. Fielding, S. Bose, *Acta Biomater.* **9**, 9137 (2013).
59. R. Detsch, S. Schaefer, U. Deisinger, G. Ziegler, H. Seitz, B. Leukers, *J. Biomater. Appl.* **26**, 359 (2010).
60. U. Klammert, T. Reuther, C. Jahn, B. Kraski, A.C. Kübler, U. Gbureck, *Acta Biomater.* **5**, 727 (2009).
61. P. Habibovic, U. Gbureck, C.J. Doillon, D.C. Bassett, C.A. van Blitterswijk, J.E. Barralet, *Biomaterials* **29**, 944 (2008).
62. J.A. Inzana, D. Olvera, S.M. Fuller, J.P. Kelly, O.A. Graeve, E.M. Schwarz, S.L. Kates, H.A. Awad, *Biomaterials* **35**, 4026 (2014).
63. B.M. Holzapfel, J.C. Reichert, J.-T. Schantz, U. Gbureck, L. Rackwitz, U. Nöth, F. Jakob, M. Rudert, J. Groll, D.W. Hutmacher, *Adv. Drug Deliv. Rev.* **65**, 581 (2013).

64. M.H. Alkhraisat, C. Rueda, L.B. Jerez, F. Tamimi Mariño, J. Torres, U. Gbureck, E. López-Cabarcos, *Acta Biomater.* **6**, 257 (2010).
65. F. Tamimi, J. Torres, U. Gbureck, E. López-Cabarcos, D.C. Bassett, M.H. Alkhraisat, J.E. Barralet, *Biomaterials* **30**, 6318 (2009).
66. J. Torres, F. Tamimi, M.H. Alkhraisat, J.C. Prados-Frutos, E. Rastikerdar, U. Gbureck, J.E. Barralet, E. López-Cabarcos, *J. Clin. Periodontol.* **38**, 1147 (2011).
67. F. Tamimi, J. Torres, K. Al-Abedalla, E. López-Cabarcos, M.H. Alkhraisat, D.C. Bassett, U. Gbureck, J.E. Barralet, *Biomaterials* **35**, 5436 (2014).
68. D. Arcos, M. Vallet-Regí, *Acta Mater.* **61**, 890 (2013).
69. J. Barralet, U. Gbureck, P. Habibovic, E. Vorndran, C. Gerard, C.J. Doillon, *Tissue Eng. Part A* **15**, 1601 (2009).
70. A. Sudo, M. Hasegawa, A. Fukuda, A. Uchida, *J. Arthroplasty* **23**, 145 (2008).
71. A. Uchida, Y. Shinto, N. Araki, K. Ono, *J. Orthop. Res.* **10**, 440 (1992).
72. P. Wu, D.W. Grainger, *Biomaterials* **27**, 2450 (2006).
73. U. Gbureck, E. Vorndran, F.A. Müller, J.E. Barralet, *J. Control. Release* **122**, 173 (2007).
74. M. Cornelsen, S. Petersen, K. Dietsch, A. Rudolph, K. Schmitz, K. Sternberg, H. Seitz, *Biomed. Tech.* **58** (Suppl. 1) (2013).
75. S.T. Becker, H. Bolte, K. Schünemann, H. Seitz, J.J. Bara, B.E. Beck-Broichsitter, P.A.J. Russo, J. Wiltfang, P.H. Warnke, *Int. J. Oral Maxillofac. Surg.* **41**, 1153 (2012).
76. S. Tarafder, S. Bose, *ACS Appl. Mater. Interfaces* **6**, 9955 (2014).
77. S. Tarafder, K. Nansen, S. Bose, *Mater. Sci. Eng. C* **33**, 3121 (2013).
78. D.M. Saylor, C.-S. Kim, D.V. Patwardhan, J.A. Warren, *J. Pharm. Sci.* **98**, 169 (2009).
79. N. Sandler, A. Määttänen, P. Ihalainen, L. Kronberg, A. Meierjohann, T. Viitala, J. Peltonen, *J. Pharm. Sci.* **100**, 3386 (2011).
80. B.M. Wu, S.W. Borland, R.A. Giordano, L.G. Cima, E.M. Sachs, M.J. Cima, *J. Control. Release* **40**, 77 (1996).
81. W.E. Katstra, R.D. Palazzolo, C.W. Rowe, B. Giritlioglu, P. Teung, M.J. Cima, *J. Control. Release* **66**, 1 (2000).
82. W. Wu, Q. Zheng, X. Guo, W. Huang, *J. Wuhan Univ. Technol. Mater. Sci. Ed.* **24**, 977 (2009).
83. D.G. Yu, L.-M. Zhu, C.J. Branford-White, X.L. Yang, *J. Pharm. Sci.* **97**, 3666 (2008).
84. D.G. Yu, X.L. Yang, W.D. Huang, J. Liu, Y.G. Wang, H. Xu, *J. Pharm. Sci.* **96**, 2446 (2007).
85. W. Wu, Q. Zheng, X. Guo, J. Sun, Y. Liu, *Biomed. Mater.* **4**, 065005 (2009).
86. D.-G. Yu, C. Branford-White, Z.-H. Ma, L.-M. Zhu, X.-Y. Li, X.-L. Yang, *Int. J. Pharm.* **370**, 160 (2009).
87. E. Vorndran, U. Klammert, A. Ewald, J.E. Barralet, U. Gbureck, *Adv. Funct. Mater.* **20**, 1585 (2010).
88. W.C. Wilson, T. Boland, *Anat. Rec. A. Discov. Mol. Cell. Evol. Biol.* **272A**, 491 (2003).
89. T. Xu, C.A. Gregory, P. Molnar, X. Cui, S. Jalota, S.B. Bhaduri, T. Boland, *Biomaterials* **27**, 3580 (2006).
90. T. Xu, J. Jin, C. Gregory, J.J. Hickman, T. Boland, *Biomaterials* **26**, 93 (2005).
91. T. Boland, T. Xu, B. Damon, X. Cui, *Biotechnol. J.* **1**, 910 (2006).
92. M.D. Weir, H.H.K. Xu, C.G. Simon, *J. Biomed. Mater. Res. Part A* **77A**, 487 (2006).
93. J. Will, R. Melcher, C. Treul, N. Travitzky, U. Kneser, E. Polykandriotis, R. Horch, P. Greil, *J. Mater. Sci. Mater. Med.* **19**, 2781 (2008).
94. J. Suwanprateeb, R. Sanngam, T. Panyathanmaporn, *Mater. Sci. Eng. C* **30**, 610 (2010).
95. H. Seitz, U. Deisinger, B. Leukers, R. Detsch, G. Ziegler, *Adv. Eng. Mater.* **11**, B41 (2009).
96. G.A. Fielding, A. Bandyopadhyay, S. Bose, *Dent. Mater.* **28**, 113 (2012).
97. C. Bergmann, M. Lindner, W. Zhang, K. Koczur, A. Kirsten, R. Telle, H. Fischer, *J. Eur. Ceram. Soc.* **30**, 2563 (2010).
98. R. Meszaros, R. Zhao, N. Travitzky, T. Fey, P. Greil, L. Wondraczek, *Glass Technol.: Eur. J. Glass Sci. Technol. Part A* **52**, 111 (2011). □